R. Güther and S. Kusch *

Transformations, multiple Filtering and associative Processes in thick Media for continuous Image Structures**

Starting with the kinematical theory (1st Borns approximation of the scattering problem) we obtain a simple formula which contains multiple filtering and associative processes including angular and wavelength coding. This formula is analyzed for a numerical comparison between thin and thick holograms in relation to the signal-to-noise-ratio. There are advantages in the signal-to-noise-ratio both for multiple filtering and associative processes for thick holograms.

1. Introduction

The associative properties of thin holograms were treated in many papers on optical filtering. In a clear way GABOR [1] depicts the associative properties of thin holograms. The influence of Bragg reflection properties of thick holograms on the correlation peak was treated in [2]. Associative combinations of discrete waves in thin and thick holograms were considered in [3] and [4]. The present paper is devoted to the influence of the volume effect in thick media on the transformation possibilities and the associative properties and to the possibilities of quantitative improvements by changing the thickness of the medium. The starting point of our calculations is the kinematical theory, that means a summation of all spherical waves produced inside the volume hologram by the reconstruction wave in the far field. The method of the kinematical theory was applied e.g. in [5] and [6].

2. General formulation of the problem

We assume N records in an ideal linear medium. For the n-th record the signal wave S, and the reference wave R are represented by superpositions of plane waves in the following form

$$S(n, r) = \iint de_s^2 \, S(n, e_s) q_s(|r \times e_s|) \exp(ik_n e_s r), \quad (1)$$

$$R(n, r) = \iint de_R^2 \, R(n, e_R) q_R(|r \times e_R|) \exp(ik_n e_R r), \quad (2)$$

where $S(n, e_S)$ is the amplitude distribution along the direction of the unit vector e_S, q_S is a function describing the cross-section of the beam, and

$$k_n = \frac{2\pi}{\lambda_n},$$

λ_n being the wavelength of the n-th record. If in a concrete case e_S is replaced by two angles Θ_S and Φ_S, as it is explained in Fig. 1a, then the integration

$$\iint de_S^2$$

takes the form

$$\int d\Phi_S \int d\Theta_S \cos\Theta_S$$

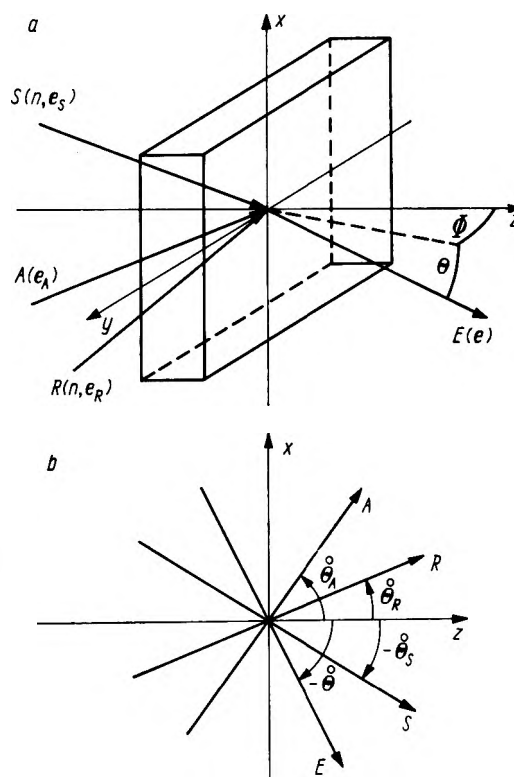according to the integration over a spherical surface (see [8], chapter 11.7).

Fig. 1. a. Geometrical configuration of the record with R and S and of the readout of the output E by A;
b — The definition of the signs of the angles

* The authors are with the Zentralinstitut für Optik und Spektroskopie der AdW der DDR, 1199 Berlin-Adlershof, Rudower Chaussee 5, DDR.

In the above substitution the symbol for S remains unchanged. The reconstruction beam is described by

$$A(r) = \int\int de_A^2 A(e_A)q_A(|r \times e_A|)\exp(ike_A r). \quad (3)$$

In the case of colour coding $k = k_m$ and $k_m \neq k_n$ for $m \neq n$. The reconstructed virtual image is given by

$$E_{\text{rec}}(e) \sim \sum_{n=1}^{N}\frac{1}{r}\int\int de_A^2 \int\int de_S^2 \int\int de_R^2 A(e_A) \times$$

$$\times S(n, e_S)R^*(n, e_R)G(e', e_A, e_S, e_R, V) \quad (4)$$

with the transfer function

$$G(e', e_A, e_S, e_R, V) = \iiint_{\substack{\text{volume } V \text{ of}\\ \text{the hologram}}} dr^3\, e^{ike'r}q_A(|r \times e_A|)q_S(|r \times e_S|) \times q_R(|r \times e_R|), \quad (5)$$

$$e' = -e + e_A + \frac{k_n}{k}e_S - \frac{k_n}{k}e_R.$$

(4) being the far field approximation of $\iiint\limits_{V}$ (induced refractive index change, recorded by S and R) x (readout wave A) x $\dfrac{\exp(ikr)}{r}\,dV$

where r is the distance between dV and the point at which the signal is detected. This is the procedure of the kinematical theory. For parallelepiped holograms (the respective dimensions along the x-, y- or z-direction being a, b or c) equation (5) results in

$$G = abc\,\text{sinc}\,\frac{ke'_x a}{2}\,\text{sinc}\,\frac{ke'_y b}{2}\,\text{sinc}\,\frac{ke'_z c}{2}, \quad (6)$$

where $\text{sinc}\,x = (\sin x)/x$, and for an infinite extended medium with a hologram made by Gaussian beams [6] in

$$G \sim \exp\left(-\frac{k}{2}e'a\right), \quad (7)$$

where the vector a depends on the recording configuration, a was given in [6].

Let us now substitute all unit vectors by the angles from Fig. 1. E.g.

$$e_x = \sin\Theta \qquad -\frac{\pi}{2} \leqslant \Theta \leqslant \frac{\pi}{2} \quad (8)$$

$$e_y = \cos\Theta\sin\Phi \quad -\frac{\pi}{2} \leqslant \Phi \leqslant \frac{\pi}{2}$$

$$e_z = \cos\Theta\cos\Phi$$

From (6) and (7) we calculate the "linear approximated" transfer functions for small angular ranges of Θ and Φ. We develop, for example, the arguments of (6) in $\overset{\circ}{\Phi}$ and $\overset{\circ}{\Theta}$ (centres of the images). Fig. 1b shows the centres of the images:

$$\Theta_S = -\overset{\circ}{\Theta}_S + \vartheta_S;\ \Phi_S = \varphi_S$$

($\overset{\circ}{\Phi}_S = 0$, since all rotations are assumed to be around the y-axis); $\overset{\circ}{\Theta}_R = \Theta_R + \vartheta_R$;

$$\Phi_R = \varphi_R;\ \Theta_A = \overset{\circ}{\Theta}_R + \vartheta_A;\ \Phi_A = \varphi_A;$$

$$\Theta = -\overset{\circ}{\Theta}_S + \vartheta;\ \Phi = \varphi.$$

Small Greek letters denote small parameters. Another small parameter $\Delta k_n = k_n - k$, describes colour coding. In the expansion of e' only first order (linear) coefficients of small parameters are taken into account. E.g. in $\Delta k_n \cdot \varphi \approx 0$, image magnification is neglected because of the change in the wavelength. From (6) we get

$$G = abc\,\text{sinc}\,\frac{ak}{2}\left\{[\vartheta_S - \vartheta]\cos\overset{\circ}{\Theta}_S + [\vartheta_A - \vartheta_R]\cos\overset{\circ}{\Theta}_R - \frac{\Delta k_n}{k}(\sin\overset{\circ}{\Theta}_S + \sin\overset{\circ}{\Theta}_R)\right\}\,\text{sinc}\,\frac{bk}{2}\{[\varphi_S - \varphi]\cos\overset{\circ}{\Theta}_S + [\varphi_A - \varphi_R] \times$$

$$\times \cos\overset{\circ}{\Theta}_R\}\text{sinc}\,\frac{ck}{2}\left\{[\vartheta_S - \vartheta]\sin\overset{\circ}{\Theta}_S + [\vartheta_R - \vartheta_A]\sin\overset{\circ}{\Theta}_R + \frac{\Delta k_n}{k}(\cos\overset{\circ}{\Theta}_S - \cos\overset{\circ}{\Theta}_R)\right\}. \quad (9)$$

From (7) for $\Delta k_n = 0$ we obtain

$$G = \frac{\pi^{3/2}\sigma^3}{\sqrt{6}}\exp\left\{-\frac{k^2\sigma^2}{8}\left[[\vartheta_A - \vartheta_R]^2 + 2[-\vartheta + \vartheta_S]^2 + \frac{2}{3}[[\varphi_S - \varphi]\cos\overset{\circ}{\Theta}_S + [\varphi_A - \varphi_R]\cos\overset{\circ}{\Theta}_R]^2\right]\right\}, \quad (10)$$

where σ is the width of the Gaussian beams.

In the sequel we discuss particular cases of the general formula, represented by the combination of (4) with (9).

3. Infinite extended volume holograms and transformations

To emphasize the character of volume holograms we assume infinite extended holograms. This means that a, b, $c \to \infty$ for parallelepiped holograms and $\sigma \to \infty$ for holograms formed by Gaussian beams. In both the cases we obtain ($\Delta k_n = 0$)

$$G = \text{const}\cdot\delta(\vartheta_A - \vartheta_R)\delta(-\vartheta + \vartheta_S)\delta(\sin\overset{\circ}{\Theta}_S[\varphi - \varphi_S] + \sin\overset{\circ}{\Theta}_R[\varphi_A - \varphi_R]). \quad (11)$$

Along the ϑ-direction the volume effect leads to two δ-functions, where for $c = 0$ (thin hologram) only a single δ-function occurs with the argument

$$([-\vartheta+\vartheta_S]\cos\overset{\circ}{\Theta}_S+[\vartheta_A-\vartheta_R]\cos\overset{\circ}{\Theta}_R).$$

Along the φ-direction a single δ-function occurs for thin and thick media. By combining (11) with (4) using a simplified notation for shortening the lengthy expressions and neglecting the n-summation we get for the "ϑ-direction parts" of all functions

$$E_{\text{rec.,thick}}(y) = S(y) \cdot A*R^*(0), \qquad (12)$$

and

$$E_{\text{rec.,thin}}(y) = \int dx\, S(x+y)A*R^*(x) \qquad (13)$$

for $c = 0$. The symbol $*$ denotes the correlation:

$$f*g(x) = \int f(y)g(y+x)\,dy.$$

The structure of (13) is also obtained for the "φ-direction parts" of all functions. In the ϑ-direction the signal is constituted by the correlation between A and R at zero; in thin media an additional integration is given.

This leads to the conclusions:

Thin media: If A is the right structure, but translated, then a translation of S occurs.

Thick media: If A is the right structure and has the right position, the correct S results.

The behaviour of the hologram perpendicularly to the direction of Bragg-vectors (φ-direction) is like that of a thin hologram.

Now we treat the transformation property of a volume hologram. If we take in (4) signal waves of equal intensity

$$S(n, \Theta) \sim \delta(\vartheta_S - \vartheta_{Sn})$$

(ϑ_{Sn} equidistant), and pass to the continuum for the n-sum ($n \to \xi$), we obtain in a simplified manner

$$E(\vartheta) \sim \int d\xi\, G(\xi, \vartheta) A(\xi); \quad G(\xi, \vartheta) = R^*(\xi, \vartheta). \quad (14)$$

For $c = 0$ or for the φ-direction the same procedure results in

$$E(\vartheta) \sim \int d\xi\, G(\xi-\vartheta)A(\xi), \qquad (15)$$

Conclusion:

Compared with thin holograms (15) thick holograms permit a more general class of transformations (14) which are general linear functionals.

Yet the practical performance of these transformation holograms must be made by a sandwich-like multiple storage of images.

The specializations of (14) are:

1. E discrete, A discrete: Transformation by a matrix G and multiple storage of information.

2. E discrete, A continuous: Multiple filtering process.

3. E continuous, A discrete: Multiple storage of images.

4. E continuous, A continuous: Transformation by a linear functional.

4. Volume holograms of finite thickness

Since the φ-direction parts of the functions are identical for thick and thin media, we discuss a two-dimensional model for the ϑ-direction parts only. The y- (φ-) coordinate of all functions is omitted. We introduce new function symbols, e.g.

$$\tilde{S}(n, \vartheta_S-\vartheta_{Sn}) = S(n, -\overset{\circ}{\Theta}_S+\vartheta_S-\vartheta_{Sn})$$

which means: The common centre of all recorded signal waves S is $\overset{\circ}{\Theta}_S$. The function $\tilde{S}$ is related to this centre. ϑ_{Sn} describes the translation of the $\tilde{S}$-structure during different records by discrete steps.

The functions

$$\tilde{R}(n, \vartheta-\vartheta_{Rn}) = R(n, \overset{\circ}{\Theta}_R+\vartheta-\vartheta_{Rn})$$

are also provided for discrete steps of translation. From (4) and (9) we get

$$E(\vartheta) \sim \sum_{n=1}^{N} \int d\vartheta_A \int d\vartheta_S \int d\vartheta_R \tilde{A}(\vartheta_A)\tilde{S}(n, \vartheta_S-\vartheta_{Sn})\tilde{R}^*(n, \vartheta_R-\vartheta_{Rn}) \times$$

$$\times \operatorname{sinc}\frac{ak}{2}\left\{[\vartheta_S-\vartheta]\cos\overset{\circ}{\Theta}_S+[\vartheta_A-\vartheta_R]\cos\overset{\circ}{\Theta}_R-\frac{\Delta k_n}{k} \times\right.$$

$$\times [\sin\overset{\circ}{\Theta}_S+\sin\overset{\circ}{\Theta}_R]\left.\right\} \operatorname{sinc}\frac{ck}{2}\left\{[\vartheta_S-\vartheta]\sin\overset{\circ}{\Theta}_S+[\vartheta_R-\vartheta_A]\sin\overset{\circ}{\Theta}_R+\frac{\Delta k_n}{k}[\cos\overset{\circ}{\Theta}_S-\cos\overset{\circ}{\Theta}_R]\right\}. \qquad (16)$$

All unessential constants preceding integral signs were omitted, $\cos\overset{\circ}{\Theta}_A, \cos\overset{\circ}{\Theta}_R$ and $\cos\overset{\circ}{\Theta}_S$ including, since they result from an approximation of the cosines of the volume element. By assuming $a \gg c$, we can devel-

op the function $\operatorname{sinc}(ck)/2\{\ldots\}$ at that ϑ_A-value which belongs to the zero of the argument of $\operatorname{sinc}(ak)/2\{\ldots\}$ Comparing the maxima of $\operatorname{sinc}(ck)/2\{\ldots\}$ with the maxima of its first derivative we see that $\operatorname{sinc}(ck)/2\{\ldots\}$

as a slowly varying function can be put before the ϑ_A-integration. The part of (16) relating to the ϑ_A-integration is

$$\int d\vartheta_A \tilde{A}(\vartheta_A)\,\mathrm{sinc}\,\frac{ak}{2}\{\ldots\} = \tilde{A}(x)*\mathrm{sinc}\,\frac{ak\cos\overset{\circ}{\Theta}_R}{2}\,x\left\{\frac{1}{\cos\overset{\circ}{\Theta}_R}\times\right.$$

$$\left.\times\left[[\vartheta_S-\vartheta]\cos\overset{\circ}{\Theta}_S-\vartheta_R\cos\overset{\circ}{\Theta}_R-\frac{\Delta k_n}{k}[\sin\overset{\circ}{\Theta}_S+\sin\overset{\circ}{\Theta}_R]]\right\}, \quad (17)$$

where x denotes the arguments of the two functions to be correlated. The brackets include the resulting argument of the correlation.

Conclusion:

If we use $\tilde{A}$ in the following, then, except for the formula after (18) (with three*), this means a correlation between $\tilde{A}$ and the point transmission function of the tranversal aperture a of the hologram. If the extention μ of the details of $\tilde{A}$ is greater than $2\lambda/a$, then $\mathrm{sinc}\,ak/2\{\ldots\}$ can be neglected (for example $a \to \infty$). If $\mu < 2\lambda/a$ then $\mathrm{sinc}(ak)/2\{\ldots\}$ can be also omitted increasing the μ of $\tilde{A}$ until $2\lambda/a$.

Taking this into account and supposing $\vartheta_{Rn} = 0$ we obtain from (16)

$$E(\vartheta) \sim \sum_{n=1}^{N}\int d\xi\,\tilde{S}(n,\xi)\,\mathrm{sinc}\,\frac{ck}{2}\left\{\frac{\sin(\overset{\circ}{\Theta}_R+\overset{\circ}{\Theta}_S)}{\cos\overset{\circ}{\Theta}_R}\left[-\vartheta+\xi+\vartheta_{Sn}-\frac{\Delta k_n}{k}\tan\left(\frac{\overset{\circ}{\Theta}_R+\overset{\circ}{\Theta}_S}{2}\right)\right]\right\}\times$$

$$\times\tilde{A}*\tilde{R}(n)\left\{\frac{\cos\overset{\circ}{\Theta}_S}{\cos\overset{\circ}{\Theta}_R}\left[-\vartheta+\xi+\vartheta_{Sn}-\frac{\Delta k_n}{k}\frac{\sin\overset{\circ}{\Theta}_R+\sin\overset{\circ}{\Theta}_S}{\cos\overset{\circ}{\Theta}_S}\right]\right\}. \quad (18)$$

This formula will be discussed in the sequel. $\vartheta_{Sn} = 0$ denotes colour coding, and $\Delta k_n = 0$ denotes angular coding.

Conclusion:

The general correlation structure of the reconstructed field is without exact arguments

$$E \sim \tilde{S}*\left\{\mathrm{sinc}\,\frac{ck}{2}(\ldots)\cdot\tilde{R}*\left[\tilde{A}*\mathrm{sinc}\,\frac{ak}{2}(\ldots)\right]\right\}.$$

The main difference between thick and thin holograms $(c = 0)$ comes from the thickness dependent factor $\mathrm{sinc}(ck)/2(\ldots)$ which cuts off the correlation between R^* and A.

Statistical phases with equiphased ranges smaller than the details μ of $\tilde{A}$, $\tilde{R}$ and $\tilde{S}$ (cf. Fig. 2) can be introduced by setting, for example,

$$\tilde{A} = \overset{\approx}{A}\exp\left(i\varphi_A(\vartheta_A)\right)$$

in (18) and calculating the intensity from (18). Here different phase statistics are assumed for all $\tilde{A}$, $\tilde{R}$ and $\tilde{S}$. If $\ll\ldots\gg$ denotes a statistical mean procedure in the

sense of [9] and [10], then for

$$\overset{\approx}{A}\ll\exp\left\{i\left(\varphi_A(\vartheta_A)-\varphi_A(\vartheta_A')\right)\right\}\gg\;\sim\delta(\vartheta_A-\vartheta_A')$$

must be employed and the same procedure must be done with other indices for $\tilde{S}$ and $\tilde{R}$.

Conclusion:

For statistical phases in (18) all field strengths must be replaced by the intensities and the sinc-functions by sinc^2. Statistical phases can be realized by statistical phase masks known from the optical storage technique.

5. Multiple filters

The adaptation of (18) to multiple filters requires $\tilde{S}(n,\xi) \Rightarrow \delta(\xi)$. The translation of $\tilde{S}$ by ϑ_{Sn} was already performed by a substitution written in the other parts of (18).

Then we obtain a pure angular coding for

$$E(\vartheta) \sim \sum_{n=1}^{N}\mathrm{sinc}\,\frac{ck}{2}\left\{\frac{\sin(\overset{\circ}{\Theta}_R+\overset{\circ}{\Theta}_S)}{\cos\overset{\circ}{\Theta}_R}\,\Delta\vartheta_{Sn}\right\}\tilde{A}*\tilde{R}^*(n)\left\{\frac{\cos\overset{\circ}{\Theta}_S}{\cos\overset{\circ}{\Theta}_R}\,\Delta\vartheta_{Sn}\right\} \quad (19)$$

with $\Delta\vartheta_{Sn} = -\vartheta + \vartheta_{Sn}$ being the difference between the detecting position ϑ and the position of the centre of $\tilde{S}(n)$. Again we see the cut-off of the correlation $\tilde{A} * \tilde{R}^*$ by the sinc-function, as shown in [2].

Conclusion:

The translation of the structure $\tilde{A}$ (to be tested) results in a translation of the correlation peak only within the range which is allowed by the thickness c of the hologram.

The conclusion in chapter 4 concerning the phase statistics is valid.

By supposing $c \to \infty$ ("very thick" medium) in (19) we obtain for the sinc-function a δ-function which fixes the argument of the correlation function $\tilde{A} * \tilde{R}^*$ to the zero value. Therefore the use of the infinitely thick medium is equivalent to putting two masks (the structures to be compared with each other) one upon the other.

Assuming, that during the recording process all $\tilde{S}(n)$ point the same direction ($\vartheta_{Sn} = 0$) and that only the colour is changed, we can derive from (18) a formula very similar to (19). If we are interested in $E(\vartheta = 0)$ (for example, signal-to-noise-ratio at the position of the correlation peak) the $E(\vartheta = 0)$ of colour coding can be derived from (19) by the following substitutions

$$\Delta\vartheta_{Sn} \Rightarrow \frac{\Delta k_{Sn}}{k} \frac{\sin\overset{\circ}{\Theta}_R + \sin\overset{\circ}{\Theta}_S}{\cos\overset{\circ}{\Theta}_S}$$

$$C \Rightarrow C\frac{\cos\overset{\circ}{\Theta}_S}{\cos\overset{\circ}{\Theta}_R + \cos\overset{\circ}{\Theta}_S}.$$

(20)

Conclusion:

Angular coding and colour coding lead to the same readout structure in the linear approximation used here.

Our main intention is a general comparison between thin and thick holograms without relation to special structures to be recognized (for example special letters). Consequently in this and the next two chapters we suppose stationary random functions [7] for A and R. Fig. 2a shows an example of such a function. The rectangular "pulses" of the ordinate value 1 are distributed over the length l with the probability $\bar{p}$ for the ordinate value 1. The width μ is a measure of the extention of the details in the image. Fig. 2b and Fig. 2c show the correlation for such functions, provided that the probabilities are statistically independent.

Now we assume the maximum angular range w_{max} available for the detection of the N signal directions, connected with the $\tilde{S}(n)$ and with an angular distance $\Delta\vartheta$ between the neighbouring directions. Then the number of filters N decreases with increasing $\Delta\vartheta$,

until the high value of $\Delta\vartheta$ forbids more than one filter. Another characteristic parameter is p_S which gives the probability that the neighbouring filters of the selected filter contain just the same or very similar
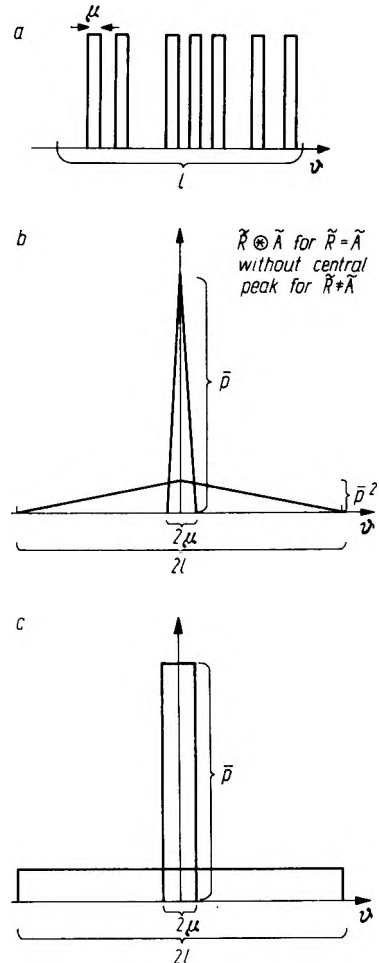

Fig. 2. a. A stationary random function, used for A and R; b. The correlation of two stationary random functions. c. Approximated correlation for simplification of the calculations

filter structure. The filter selected, for which the signal-to-noise-ratio for the reconstruction is calculated, lies in the middle of the filters, since at this position the greatest noise is expected. The signal is defined by the expression (19), it has only the central peak shown in Fig. 2c for the selected filter structure. The noise at the peak contains:

1. The function of Fig. 2c without the central peak for the selected filter ($\tilde{A} \neq \tilde{R}$).

2. The noise contribution (without peak) from the correlation functions relating to the other filters.

3. The peaks of the other correlation functions multiplied by the probability p_S, because not every filter corresponds (for example with great similarity) to the selected filter.

To catch the maximum noise we take for sinc x the function $|\text{sinc } x|$. After squaring we obtain the

intensities for the calculation of the signal-to-noise-ratio. Figs. 3 and 4 show examples of this treatment calculated by a small computer. The fixed values for all plots are: $w_{max} = 0.8$; $l = 0.3$; $p_S = 0.2$; $\bar{p} = 0.1$; $\overset{\circ}{\Theta}_S = \overset{\circ}{\Theta}_R = 0.8$ and $\Delta\vartheta_{max} = 0.3$. The varying values are $c = 1$ μm, 10 μm, 100 μm, 1 mm, 1 cm, $\mu = 0.003$ in Fig. 3 and $\mu = 0.1$ in Fig. 4. Dashed lines show the changes resulting from the introduction of a phase statistics to $\tilde{A}$ and $\tilde{R}(n)$. The dotted line in Fig. 3 shows the diminishing number of filters, connected with the chosen angular distance

$\Delta\vartheta$ and fixed w_{max}. The plots show a better signal-to-noise-ratio for greater thickness. Fig. 4 for $c = 100$ μm shows the plot with sinc x (dotted line) instead of $|\text{sinc } x|$. The result are oscillations connected with coherent information processing. For all the curves it can be shown that the decrease of the SNR by using $|\text{sinc } x|$ is not greater than a factor $1.5 \ldots 2$. For $c = 1$ μm and small $\Delta\vartheta$ the case with phase statistics is better than the case without phase statistics, both with $|\text{sinc } x|$ and sinc x.
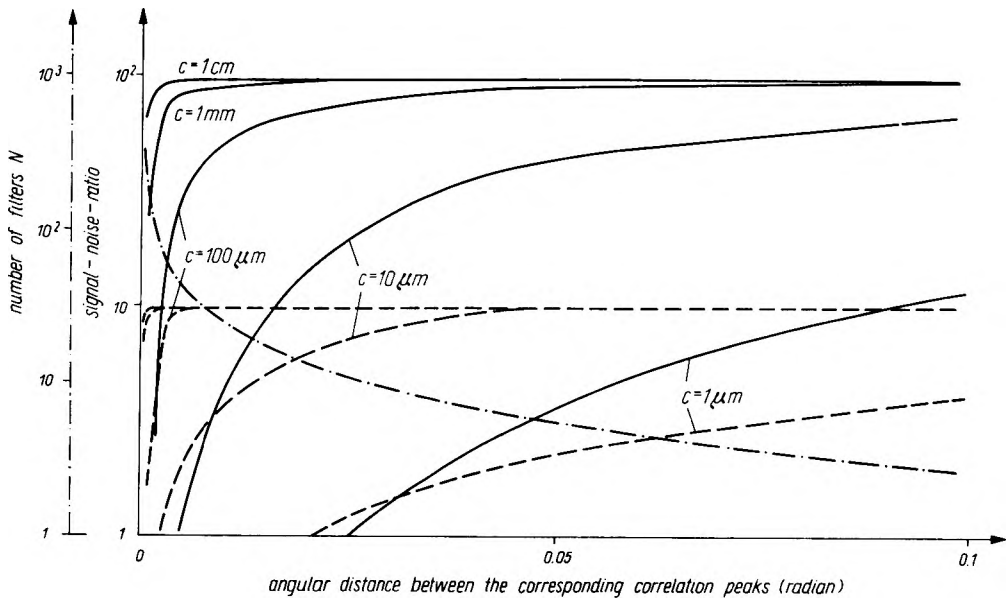

Fig. 3. Signal-to-noise-ratio of multiple filters (full lines: without statistical phases, dotted lines: with statistical phases) and the number of multiple filters for stochastic continuous function vs. the angular distance between the filters $\Delta\vartheta$ and the thickness c of the hologram with $\mu = 0.003$ radian
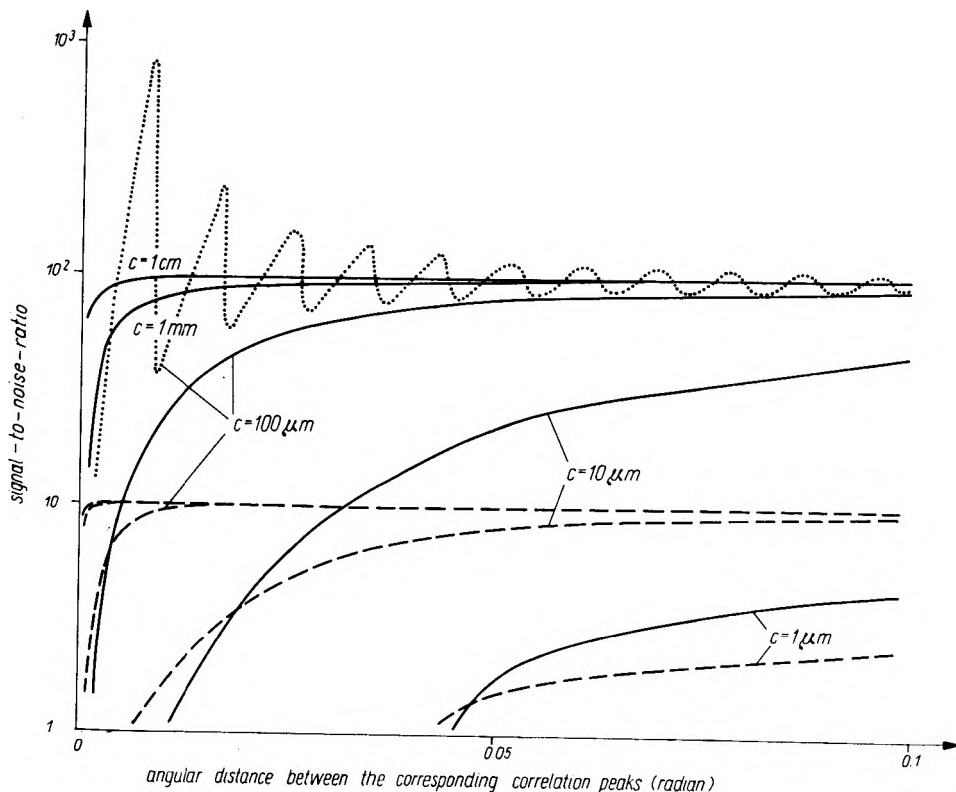

Fig. 4. Signal-to-noise-ratio, as in Fig. 3 but with $\mu = 0.1$; the dotted line shows the curve for $c = 100$ μm with sinc x instead of $|\text{sinc } x|$.

Conclusion:

The thickness leads to a better signal-to-noise-ratio. The advantage of multiple filtering is connected with the disadvantage of an additional rotation, because of the smallness of the range, determined by c, where a translation of the symbol is detected by the translation of the corresponding correlation peak.

The translation of the plots of Figs. 3 and 4 into colour coding is made by the substitutions (20) with an interpretation analogous to that given above.

6. A single associative process

This process is described by omitting the n-sum in (18)

$$E(\vartheta) \sim \int d\xi \tilde{S}(\xi) \operatorname{sinc} \frac{ck}{2} \left\{ \frac{\sin(\overset{\circ}{\Theta}_R + \overset{\circ}{\Theta}_S)}{\cos \overset{\circ}{\Theta}_R} (-\vartheta + \xi) \right\} \tilde{A} * \tilde{R} \left\{ \frac{\cos \overset{\circ}{\Theta}_S}{\cos \overset{\circ}{\Theta}_R} (-\vartheta + \xi) \right\}. \tag{21}$$

Assuming for $\tilde{S}(\xi)$ a rectangular "pulse" of the width b we obtain the signal-to-noise-ratio at $\vartheta = 0$ (the middle of the readout $E(\vartheta)$) using the approximation $\operatorname{sinc} x \approx 1$ for $0 \leqslant x \leqslant \pi/2$, and $\operatorname{sinc} x \approx 1/x$ for $\pi/2 \leqslant x$. The result is presented in Fig. 5. This
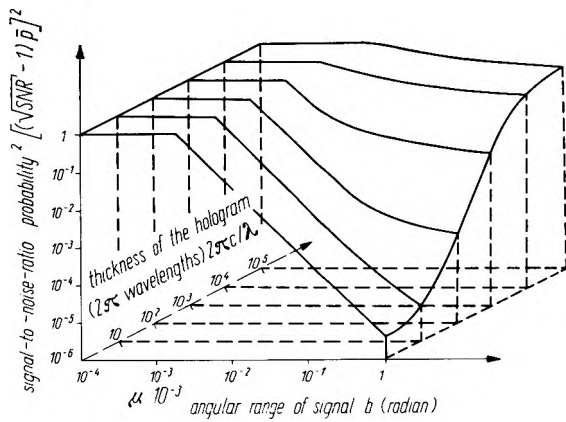

Fig. 5. Signal-to-noise-ratio of a single associative process as a function of the angular width of the signal structure, to be detected, and of the thickness of the medium

shows: If the width b of S is smaller than the "structure constant" μ, then there is a great similarity to a filtering process and volume holograms and thin holograms do not differ. For $b > \mu$ the increase in the thickness brings back the associative process to the "former filter quality".

Fig. 6 shows an obvious argument. Since equation (21) means the integration over the product of 3 functions each with "cut-off character", there must be a careful distinction between the cases where different functions cause the cut-off. If $b > \mu$ there is a better signal-to-noise-ratio for thick holograms.

Conclusion:

For "true" associative processes ($b > \mu$, S has "image character") the thick medium is advantageous.

Now we discuss the reconstruction quality of $E(\vartheta)$ of (21) outside the "ideal" $\tilde{S}$ which was recorded. For a very broad correlation function $\tilde{A} * \tilde{R} = \tilde{R} * R \approx 1$

without the assumption of stochastic processes in $\tilde{R}$ from (21) we obtain a simple expression containing
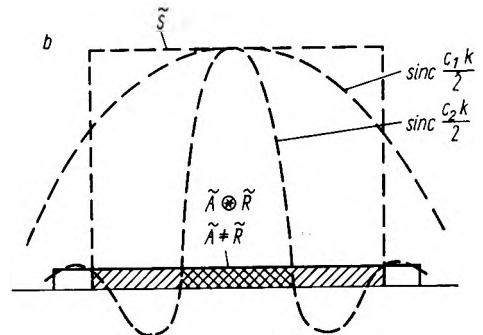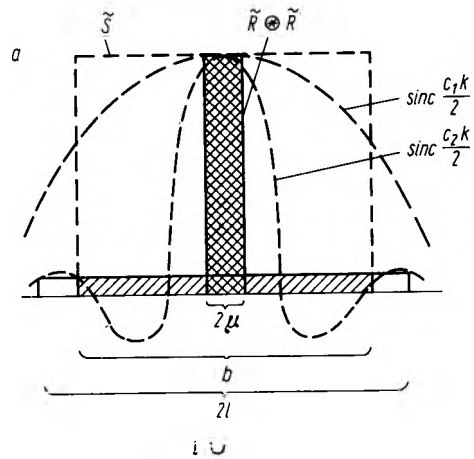
$$\int_0^x dx' \operatorname{sinc} x'$$

Fig. 6. a. Signal at two different thicknesses $c_1 < c_2$. The integral over ξ in (21) is nearly the same for both the cases

b. The noise is essentially influenced by the thickness of the medium. The double shadowed area is $\approx 1/3$ of the shadowed area. Therefore the signal-to-noise-ratio differes by the factor 3

which describes the behaviour of the reconstructed E-field near the edge of the "ideal" $\tilde{S}$, shown in Fig. 7. The noisy field outside $\tilde{S} \neq 0$ diminishes with increasing thickness.
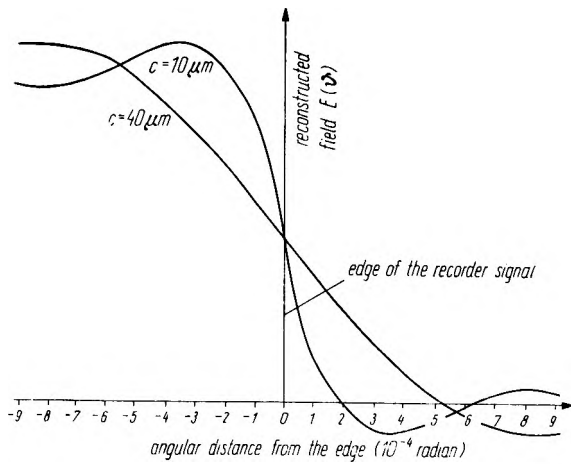
Fig. 7. Reconstructed field near the edge of the "ideal" $\tilde{S}$ (vertical line) versus the thickness, for a single associative process

7. Multiple associative processes

The formula (18) was programmed on a small computer with the same signal and noise parts as explained in chapter 5. Fig. 8 shows the case of mul-
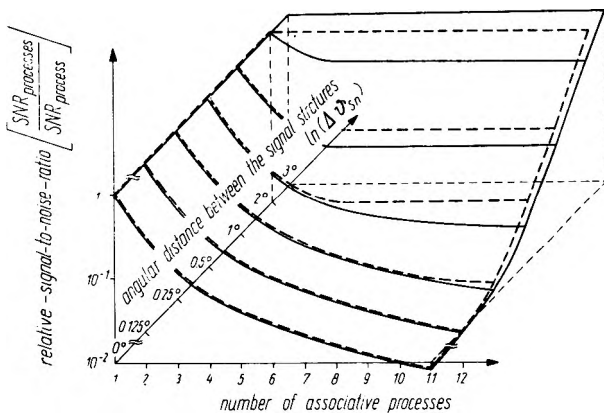

Fig. 8. Relative signal-to-noise-ratio of multiple associative processes versus the angular distances between the processes, and the number of processes. Full lines: angular coding, dashed lines: colour coding

tiple associative processes in dependence on the number of processes and on the angular distance between neighbouring processes. If all associative processes are superposed without angular distance $(\Delta\vartheta = 0)$, the signal-to-noise-ratio decreases with $1/N^2$. If the distances are great enough (i.e. the space frequencies have no lap ranges) the signal-to-noise-ratio is constant. The parameters used are $c = 10$ μm, $\overset{\circ}{\Theta}_R = \overset{\circ}{\Theta}_S = 0.8$, $\vartheta = 0$, $b = 1°$, $\mu = 0.003$ radian, $l = 2.5°$, $\Delta k_A/k_A = \Delta\vartheta_S = 0.0174$ radian, $p_S = 0$, $\bar{p} = 0.1$. The dashed plots show the colour coding, where $\Delta k_{An}/k_A$ has the same value as $\Delta\vartheta_{Sn}$, measured in radian. We see that the difference is small.

Fig. 9 shows an example for the signal-noise distribution of the reconstructed function E over the angular range of this function. This figure results from
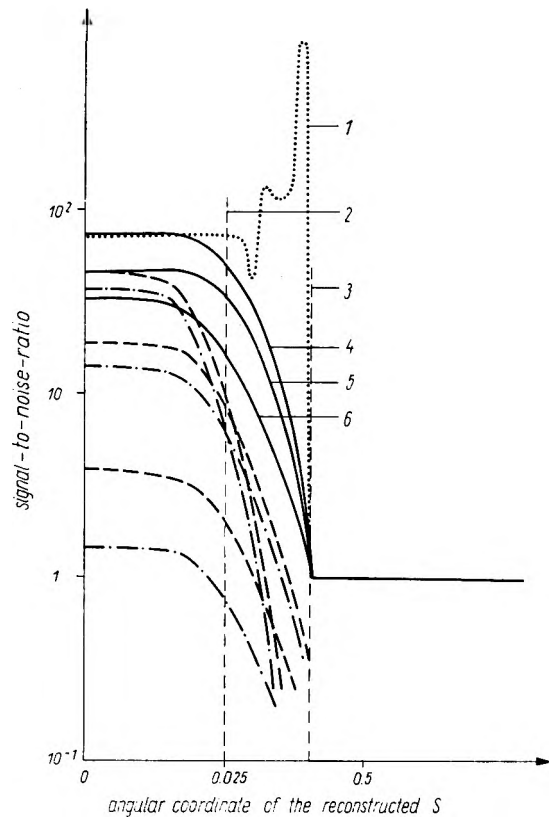

Fig. 9. Reconstructed signal-to-noise-ratio of the intensity in the ideal case a rectangular shaped pulse of the width $b = 0.05$ is to be expected. The associative process is disturbed by zero (full lines), two (dashed lines) or four (dash-dot lines) neighbouring processes. The dotted line gives the result for sinc x instead of $|\text{sinc}\,x|$.

1 — case with sinc x, *2* — edge of the recorded S, *3* — edge with μ added, *4* — $c = 50$ μm, *5* — $c = 10$ μm, *6* — $c = 1$ μm

programming equation (18) on a small computer. The parameters used are $\lambda = 6.328 \cdot 10^{-5}$ cm, $\overset{\circ}{\Theta}_R = \overset{\circ}{\Theta}_S = 0.8$, $b = 0.05$, $l = 0.3$, $\mu = 0.015$, $\Delta\vartheta_S = 0.05$, $p_S = 0$ and $\bar{p} = 0.1$. The edge of the recorded $\tilde{S}$ (a rectangular pulse of width b) is plotted. We see that the thickness improves the signal-to-noise-ratio over the whole angular range of $\tilde{S}$. The widths of the correlation $\tilde{R}*\tilde{R}$ and of $\text{sinc}(ck)/2(...)$ in (21) are responsible for SNR > 1 for ϑ-values outside the recorded S. The influence of the thickness results in an increased signal-to-noise-ratio. The dotted line was calculated with sinc x instead of $|\text{sinc}\,x|$ (see chapter 5) for the thickness 50 μm and a single associative process. The oscillations, like those in chapter 5, are obvious.

Conclusion:

For superpositions of associative processes a thick medium is also advantageous.

8. Discussion

We have shown that the topological structure of the lattice vectors in thick media enables functional transformations. The advantage of thick media for

filtering results from the better signal-to-noise-ratio for multiple filters, compared with thin media. Single and multiple associative processes are better in thick media. The results were derived for an ideal medium.

*

* *

Трансформации, многократное фильтрование и ассоциативные процессы в плотных средах для сплошных структур изображений

Исходя из кинематической теории (первые приближения Борнса для вопроса рассеяния), получают простую формулу, в которой содержатся многократное фильтрование и ассоциативные процессы, охватывающие угловое кодирование и длины волны. Формула подвергается анализу для численного сопоставления тонких и толстых голограмм по отношению к величине сигнал/шум. В толстых голограммах это величина является полным для многократного фильтрования, волны и ассоциативных процессов.

References

[1] Gabor D., IBM J. Res. Devel., 13, 56 (1969).

[2] Douklias N. and Shamir J., Appl. Opt. 12, 364 (1973); Brousseau N. and Arsenault H. H., Appl. Opt. 14, 1679 (1975).

[3] Knight G. R., Appl. Opt. 13, 904 (1974), 14, 1088 (1975); Sakaguchi M. et all., IEEE Trans. on Comp., C-19, 1174, (1970).

[4] Kusch S. and Güther R., Associativity in thick holograms, to be published.

[5] Leith E. N. et all., Appl. Opt. 5, 1303 (1966); Denisyuk J. N., Optica i Spectroscopia (Russ.), 15, 522 (1963); Ramberg E. G., RCA Review, 33, 5 (1972); Wolf E., Opt. Commun. 1, 153 (1969).

[6] Güther R. and Kusch S., Kvantovaya Electronica (Russ.), 3, No. 5 (47), 949 (1976).

[7] Jaglom A. M., An introduction to the theory of stationary random functions, Prentice Hall, Englewood Cliffs N. J., 1962.

[8] Born M. and Wolf E., Principles of optics, Oxford 1964.

[9] Kozma A. et all., Appl. Opt. 9, 721 (1970).

[10] Soroko L. M., Osnovy golografii i kogerentnoy optiki (Russ.), Moscow 1971, p. 286.